RSC Advances

ROYAL SOCIETY OF CHEMISTRY

www.rsc.org/advances

High supercapacitive performance of $Ni(OH)_2$/XC-72 composite prepared by microwave-assisted method

Shuihua Tang[1,2,*], Leping Sui[1,2], Zhen Dai[1,3], Zhentao Zhu[1,2], Haixin Huangfu[1,2]

[1]*State Key Lab of Oil and Gas Reservoir Geology & Exploitation, Southwest Petroleum University, Chengdu 610500, China*
[2]*School of Materials Science and Engineering, Southwest Petroleum University, Chengdu 610500, China*
[3]*School of Chemistry and Chemical Engineering, Southwest Petroleum University, Chengdu 610500, China*
**Corresponding author. E-mail: shuihuatang@swpu.edu.cn, Tel/Fax: +86-2883032879 (S H Tang);*

Abstract

60 wt% $Ni(OH)_2$/XC-72 composite was synthesized via a facile and rapid microwave assisted method in an ethylene glycol medium. Transmission electron microscopy images show that $Ni(OH)_2$ are uniformly dispersed on XC-72, and carbon nanotubes (CNTs) constructs a three-dimensional (3-D) network together with XC-72 and $Ni(OH)_2$ particles when CNTs is added as a conductive agent. The composite demonstrates a specific capacitance of 1296 F g^{-1} at a scan rate of 2 mV s^{-1} and 1560 F g^{-1} at a current density of 1 A g^{-1} in 6 M KOH aqueous solution, and its retention of specific capacitance is 71% after 1000 cycles. This can be attributed to XC-72 being an excellent support, and CNTs with high respect ratio and good conductivity to construct a 3-D conductive network. The excellent electrochemical performance makes $Ni(OH)_2$/XC-72 composite promising to be an electrode material for a supercapacitor.

Introduction

High efficient, environment-friendly, safe, and renewable energy sources are extremely demanded for a modern society. Supercapacitor, as an energy storage device, with advantages of high power density, long cycling life, friendly environment, and wide temperature operation window, has been drawn much attention in recent years [1-3].

Generally, based on its energy storage principles, a supercapacitor can be divided into two types. One is defined as an electrical double layer capacitor (EDLC), electrical energy is electrostatically stored at an interface between a conductive electrode and an electrolyte. Typically, commercial EDLC electrode materials are porous carbon nanomaterials such as activated carbon [4], carbon nanotubes [5, 6] and carbon aerogels [7, 8], which have advantages of large specific surface area, good electron conductivity, and stability, but still have disadvantages of low specific capacitance and energy density, which limit their applications. The other one is defined as a pseudocapacitor, electrical energy is stored by faradaic reactions such as redox reaction, intercalation, or electrosorption [9]. The most studied materials for pseudocapacitors are conducting polymers such as polyaniline [10] and transition metal oxides/hydroxides such as RuO_2 [11], MnO_2 [12, 13], Co_3O_4 [14], $Ni(OH)_2$/NiO [15], α-FeOOH [16], which always behave high specific capacitance but poor cycling stability [17-19].

Among such multitudinous materials for pseudocapacitors, $Ni(OH)_2$ has been extensively researched due to its low cost, high theoretical specific capacitance (2082 F g^{-1}), simple synthesis process and various available morphologies [1,20, 21]. However, there is a big issue lied on large particles, poor stability, and bad electron conductivity. Hence, a composite of $Ni(OH)_2$/carbon materials has been widely investigated [22-26].

Huang *et al* has synthesized $Ni(OH)_2$/activated carbon composite by chemical precipitation method. When nickel hydroxide loading was 6 wt%, the composite showed a high specific capacitance of 314.5 F g^{-1}, which was 23.3% higher than pure activated carbon (255 F g^{-1}) [4]. Chen *et al* synthesized α-$Ni(OH)_2$/ reduced graphene oxide/carbon nanotubes by one-pot hydrothermal method and found that the amount of carbon nanotubes could significantly influence its electrochemical performances. The composite with GO/CNTs mass ratio of 20:2 and concentration of $NiCl_2 \cdot 6H_2O$ is 59.5 mg mL^{-1} exhibited a specific capacitance of 1320 F g^{-1} at 6 A g^{-1} and about 7.8% of capacitance was reduced after 1000 cycles [5]. Zhang *et al* prepared a 3-D hierarchical composite of α-$Ni(OH)_2$/graphite nanosheet with introducing the graphene oxide nanosheets into α-$Ni(OH)_2$, then a 3-D hierarchical porous structure of fine α-$Ni(OH)_2$ nanocrystals as building blocks is formed directly on the matrix of graphite nanosheets in the presence of urea, exhibited a high specific capacitance of 1956 F g^{-1} at 1 A g^{-1} and the capacitance retention can reach to 70% after 1000 cycles [22]. Ji *et al* synthesized a free-standing $Ni(OH)_2$/ultrathin-graphite foam (UGF) composite, and an asymmetric supercapacitor made with $Ni(OH)_2$/UGF as positive electrode and graphite oxide as negative electrode showed a high power density of 44.0 kW kg^{-1} [23]. Wang *et al* synthesized α-$Ni(OH)_2$/carbon nanotube composite based on carbon nanotube paper, α-$Ni(OH)_2$ nanosheets were vertically grown on individual carbon nanotube to form hierarchical nanowires, the composite with this novel structure brought a high specific capacitance of 1144 F g^{-1} at 0.5 A g^{-1} [24].

Vulan XC-72 is the most widely used support for electrocatalysts in low temperature fuel cells, because of its good conductivity, large percentage of mesopores, and excellent stability. Its specific surface area is ca. 250 m^2, but metallic platinum or platinum-ruthenium particles are below 5 nm even though the metal loading reaches up to 60 wt% [27]. Till now, no related literature of XC-72 alone as an electrode material or as a support for a supercapacitor is reported. As compared to graphene or CNTs, XC-72 is a commercial product and much cheaper, and it is even cheaper than the most used activated carbon for commercial supercapacitors. In this paper, XC-72 will be used as a support to synthesize $Ni(OH)_2$/XC-72 composite in an ethylene glycol (EG) medium, in which EG will be used both as solvent and complex to obtain smaller $Ni(OH)_2$ particles. Furthermore, a more effectively microwave-assisted heating will be adopted to synthesize $Ni(OH)_2$/XC-72 composite to achieve smaller $Ni(OH)_2$ particles and uniform distribution than normal heating method. Eventually, carbon nanotubes (CNTs) will be added during the process of electrode slurry preparation, aims to construct a 3-D conductive network, thus facilitate electron transfer and enhance electrochemical stability of the composite.

Experimental

2.1 Synthesis of $Ni(OH)_2$/XC-72composite

$Ni(OH)_2$/XC-72 composite was synthesized in a medium of ethylene glycol via a fast, green, and facial microwave heating method. The typical procedure is as follows, for a 60 wt% $Ni(OH)_2$/XC-72 composite, 20 mg of Vulcan XC-72 carbon black powder from Cabot Company was dispersed in 90 mL of ethylene glycol, then 3.2 mL of $NiCl_2$ ethylene glycol solution (0.1 M) was added and stirred for 30 min, later 0.5 M NaOH ethylene glycol solution was added until the pH value reached 11.3, kept continuous agitation for another 30 min. The resulting suspension was heated in a microwave oven (Midea, MM721NH1-PW) with a power of 700 W for 3 min, followed by stirring for 10.5 h to get $Ni(OH)_2$ nanoparticles deposited on carbon black XC-72 at room temperature. Finally, the suspension was filtered, washed by distilled water several times and dried in a vacuum oven at 70°C overnight.

2.2 Characterization

Carbon black XC-72 and the as-prepared 60 wt% $Ni(OH)_2$/XC-72 composite were characterized by X-ray powder diffraction (XRD, Philips X' pert PRO MPD) with Cu Kα radiation (λ=0.15406 nm). The morphologies of the composite and the electrode slurry with added CNTs were observed on a Libra 200FE transmission electron microscopy (Carl Zeiss SMT Pte Ltd) operated at 200 kV, and the morphology of electrode before and after life tests were observed on a Zeiss EVO MA 15 scanning electron microscope. Fourier transform infrared (FTIR) spectra between 410 and 4000 cm^{-1} were obtained on a Nicolet 6700 spectrometer. Raman spectra were obtained on a Renishaw InVia Raman spectrometer with incident laser light of 514.5 nm for XC-72 and the composite, respectively.

The electrochemical performances were evaluated by cyclic voltammetry (CV), galvanostatic charge-discharge, and electrochemical impedance spectroscopy (EIS), using a 302 N AutoLab Potentiostat (Metrohm, Holland), in a three-electrode system. Nickel mesh with dimension of 10×10 was cleaned before used as a substrate of working electrode, Hg/HgO electrode as a reference electrode, platinum coil as a counter electrode, and 6 M KOH as an electrolyte. 1000 cycles of life test was carried out with a CV scan rate of 100 mV s^{-1}.

To prepare a working electrode, active materials (60 wt% $Ni(OH)_2$/XC-72 composite), conductive agent, and binder (60 wt% Polytetrafluoroethylene emulsion) were mixed with a mass ratio of 85 :10 :5 in ethanol, then ultrasonically stirred for 20 min before dropped onto a nickel foam and dried in 70 °C vacuum oven for 6 h. Eventually, the working electrode was pressed under 10 MPa for 1 min. The areal density of the active materials is 1 mg cm^{-2}. For conductive agent, acetylene black (AB) and carbon nanotubes (CNTs, Chengdu Organic Chemicals Company, China) were investigated, respectively. The obtained electrode was denoted as XC-CNT or XC-AB.

The specific capacitance of the synthesized composite can be calculated from a CV curve, using the following equation,

$$C = \int I \mathrm{d}V \Big/ 2\mathrm{m}\nu\Delta V \qquad (1)$$

Where m is mass of active materials, ν indicates scan rate, and ΔV represents voltage window.

And the specific capacitance can also be calculated from a galvanostatic charge-discharge curve based on the equation below,

$$C = I\Delta\mathrm{t}/\mathrm{m}\Delta V \qquad (2)$$

Where m also represents the mass of active material, I is current density of discharge, Δt is time of discharge, and ΔV also indicates voltage window.

Results and discussion

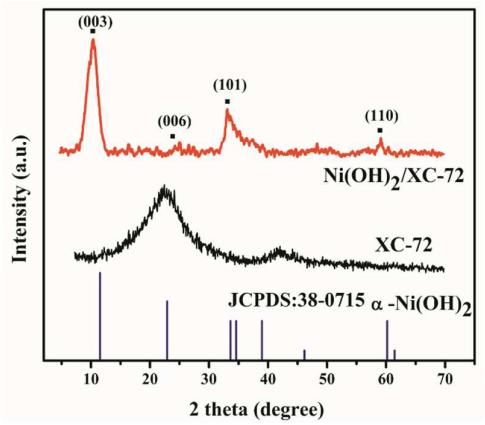

Fig. 1 XRD patterns of Ni $(OH)_2$/XC-72 composite, XC-72, and the standard spectrum of α-$Ni(OH)_2$.

XRD was performed to characterize crystalline structures. The XRD patterns of XC-72, standard spectrum of α-$Ni(OH)_2$, and $Ni(OH)_2$/XC-72 composite are illustrated in **Fig. 1**. Characteristic peaks of α-$Ni(OH)_2$ lie at 11.9°, 23.2°, 34.1°, 60.3° according to the standard spectrum of α-$Ni(OH)_2$ (referred as JCPDS NO. 38-0715), which are correspond to crystalline facets of (003), (006), (101) and (110). For $Ni(OH)_2$/XC-72 composite, three main characteristic peaks appear at 10.5°, 33.1°, 59.4°, which are very close to 11.9°, 34.1°, 60.3°, therefore can be assigned to the crystalline facets of (003), (101), and (110) of α-$Ni(OH)_2$.The average crystalline size of $Ni(OH)_2$ calculated from the (003) diffraction peak using Scherrer's formula is 13.7 nm. In addition, the characteristic peaks of XC-72 could not be observed obviously for $Ni(OH)_2$/XC-72 composite, indicating that the crystalline α-$Ni(OH)_2$ particles are dominant in the composite.

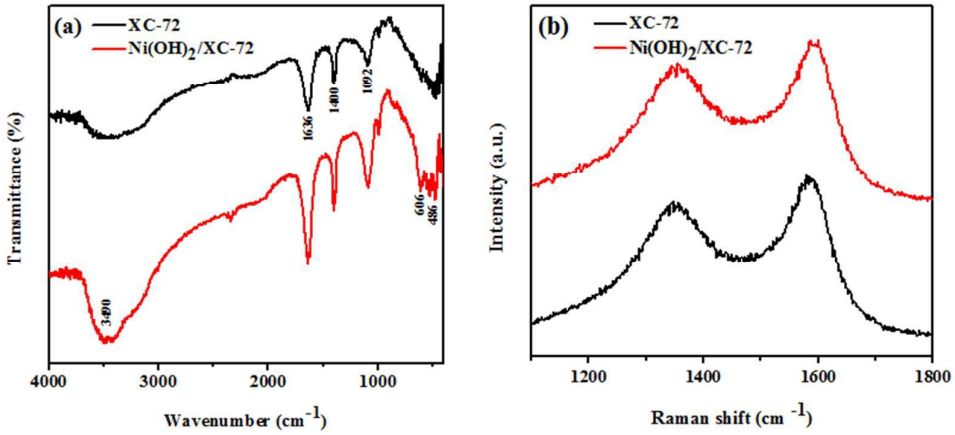

Fig. 2 FTIR (a) and Raman (b) spectra of carbon black XC-72 and $Ni(OH)_2$/XC-72 composite.

The FTIR spectra of XC-72 and $Ni(OH)_2$/XC-72 composite are shown in **Fig. 2** (a). The broad band in the range 3000-3700 cm^{-1} is assigned to O-H stretching vibration of a hydrogen-bonded water molecule. Besides, peak at 1636, 1400 and 1092 cm^{-1} are corresponded to C=C, C-OH, C-O-C vibration frequency, respectively. Other absorption bands below 800 cm^{-1} are associated with the metal-oxygen (M-O) stretching and bending models [28]. In the FTIR spectrum of $Ni(OH)_2$/XC-72 composite, the band intensity at 3490 cm^{-1} due to O-H stretching vibration are strengthened, new bands at 606 and 486 cm^{-1} are appeared, which can be attributed to the Ni-O-H bending and Ni-O stretching vibrations, respectively [29]. Therefore, the characteristic Ni-O and O-H bands of $Ni(OH)_2$ are all observed [30], then we can deduce that $Ni(OH)_2$/XC-72 composite is formed.

Raman spectra are employed to investigate the vibration properties of XC-72 and $Ni(OH)_2$/XC-72 composite. From the Raman spectra **Fig. 2** (b), they clearly show that D band around 1351 cm^{-1} and G band around 1590 cm^{-1} are included in carbon black and the composite, which are corresponded to the breathing modes of rings or k-point photons of A_{1g} symmetry and the E_{2g} vibrational mode of sp^2-bonded carbon atoms, respectively [31]. Also, the

intensity ratio of the D and G band (I_D/I_G) can be used as a useful measurement of the disorder degree and average size of the sp^2 domains of the graphite materials. From the spectra of XC-72 and $Ni(OH)_2$/XC-72 composite, the I_D/I_G ratio of $Ni(OH)_2$/XC-72 (0.87) is slightly higher than that of XC-72 (0.86), which is probably due to more presences of unpaired defects and further decrease in the average size of the sp^2 graphitic domains caused by the incorporation of $Ni(OH)_2$ [32].

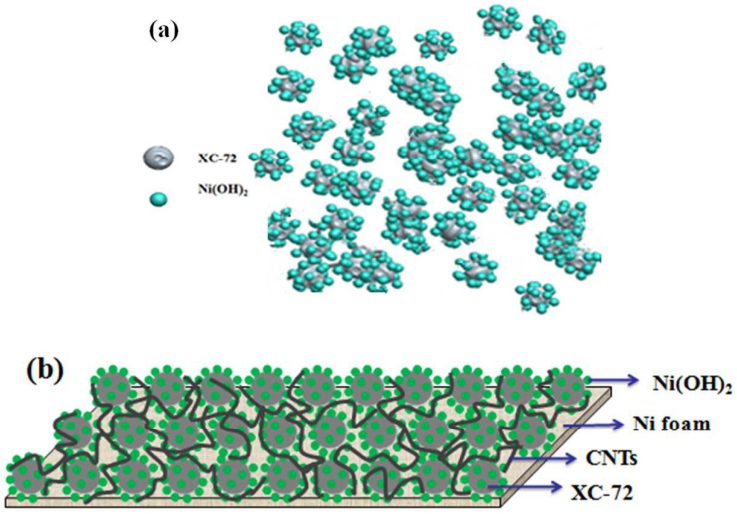

Fig. 3 Schematic structures of 60 wt% $Ni(OH)_2$/XC-72 composite (a) and XC-CNTs electrode (b), respectively.

Fig. 3 (a) implies that $Ni(OH)_2$ nanoparticles are well-distributed onto the surface of XC-72 nano-spheres, XC-72 with large specific surface area and rich meso-pores, which is regarded as an excellent support for fuel cell catalysts, then its supported $Ni(OH)_2$ particle size is supposed to be small. **Fig. 3** (b) demonstrates that the electrode with added CNTs has constructed a unique nanostructure which CNTs are cross-linked each other to form a 3-D conductive network together with $Ni(OH)_2$ and XC-72 nanoparticles. This unique structure is facilitated for electron transfer and electrolyte ions to get access to active sites, thus reduce equivalent series resistance and transfer resistance.

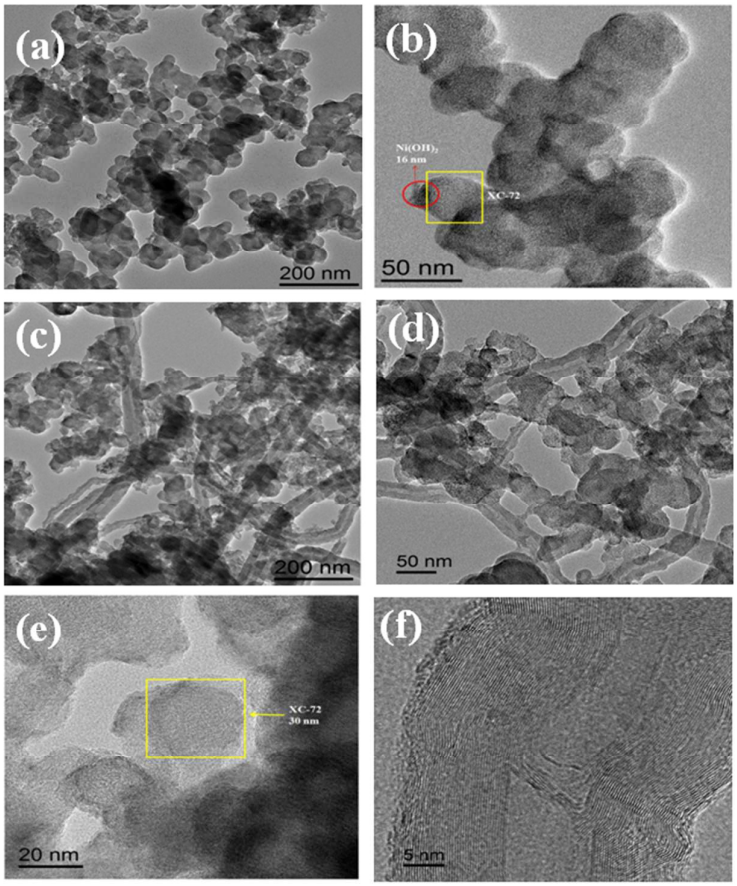

Fig. 4 HRTEM images of $Ni(OH)_2$/XC-72 composite (a, b), $Ni(OH)_2$/XC-72 electrode slurry with CNTs as conducting agent (c, d) and XC-72 (e) CNTs (f).

Typical HRTEM images of $Ni(OH)_2$/XC-72 composite are shown in **Fig. 4** (a, b). $Ni(OH)_2$ are uniformly distributed onto the surface of XC-72 nanospheres. From **Fig. 4** (c) and (d), it is evidently observed that $Ni(OH)_2$ and XC-72 nanospheres are connected by CNTs, similar to that we implied in **Fig. 3**. HRTEM images of XC-72 nanosphere with size of 30 nm and CNTs are shown in **Fig.4** (e) and **Fig. 4** (f). This unique 3-D conductive network will be expected to facilitate the ions and electrons migration, thus reduces the charging/discharging impedance, and leads to better electrochemical performances.

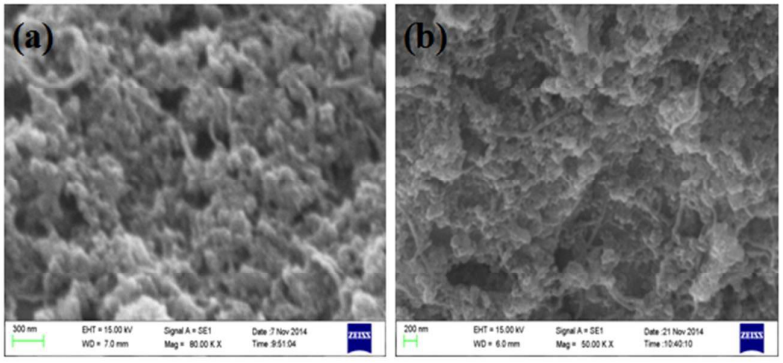

Fig. 5 SEM images of 60 wt% $Ni(OH)_2$/XC-72/CNTs electrode before (a) and after (b) 1000-cycle CV life test.

From SEM images in **Fig. 5** (a), it can be discerned that XC-72 spheres are uniformly covered by $Ni(OH)_2$. Meanwhile, CNTs are obviously existed like a network among the composite from the SEM image. The practical structure of $Ni(OH)_2$/XC-72/CNTs is in good agreement with the schematic one. After 1000 CV cycles with a scan

rate of 100 mV s^{-1}, $Ni(OH)_2$ particles can be observed to agglomerate slightly, but the composite still maintains an effective 3-D conductive net-work with $Ni(OH)_2$ and XC-72 particles connected by CNTs, therefore it can be deduced that its stability should keep well.

Electrochemical performances

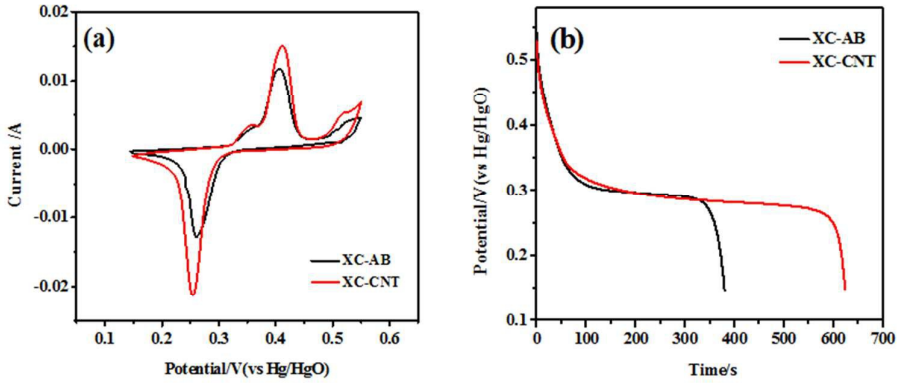

Fig. 6 Electrochemical performances of XC-AB and XC-CNT electrodes. CV curves at scan rate of 2 mV s^{-1} (a) and typical discharge curves at current density of 1 A g^{-1} (b).

The cyclic voltammograms of XC-AB and XC-CNT are shown in **Fig. 6(a)**. The anodic and cathodic potentials are respectively located at 0.41 V and 0.25 V (vs Hg/HgO reference electrode in 6 M KOH electrolyte), which can be corresponded to the oxidation and reduction potentials of the charging/discharging reaction β-$Ni(OH)_2 + OH^- \leftrightarrow \beta$-$NiOOH + H_2O + e^-$. Furthermore, besides the anodic peak of 0.41 V, there is still a shoulder peak located at ca. 0.36 V, it may be associated with the anodic reaction of α-$Ni(OH)_2$ [33-35]. β-$Ni(OH)_2$ is dominant in the composite, because the composite was dried in vacuum at 70 °C for overnight, so majority of α-$Ni(OH)_2$ will lose part interlayer water and convert into more dense β-$Ni(OH)_2$**.** The corresponding anodic and cathodic current densities are 15.1 mA cm^{-2} (I_a) and 21.1 mA cm^{-2} (I_c) for XC-CNT, and 11.8 mA cm^{-2} (I_a) and 12.6 mA cm^{-2} (I_c) for XC-AB, the values of I_a/I_c for both XC-CNT and XC-AB are equal to nearly 1, this denote that the charging/discharging reaction is reversible. . According to equation (1), the specific capacitances are calculated to be 910 F g^{-1} and 1296 F g^{-1} at scan rate of 2 mV s^{-1} for 60 wt% $Ni(OH)_2$/XC-72 when using AB and CNT as conductive agent, respectively. Both of them are much higher than 62 F g^{-1} of pure XC-72 at same scan rate of 2 mV s^{-1}. **Fig. 6** (b) depicts the galvanostatic discharge tests performed at an applied constant current density of 1 A g^{-1}. 60 wt% $Ni(OH)_2$/XC-72 composite has a potential plateau in discharge curves, and the discharge time of CNTs as conductive agent is more than 200 s longer than that of AB as conductive agent under identical conditions, the respective capacitance is 1560 F g^{-1} for the former and is 951 F g^{-1} for the latter according to equation (2), the former is ca. 60% better than the latter. If there is no conductive agent added, the $Ni(OH)_2$/XC-72 composite has a specific capacitance of 728 F g^{-1} at current density of 1 A g^{-1} as shown in **Fig. S1**, which is comparable to that with AB as conductive agent, this indicates that the conductivity of carbon black XC-72 is not bad. However, the specific capacitance is much lower than that of CNTs as conductive agent, thanks to CNTs with excellent conductivity and high respect ratio to construct a 3-D conductive net-work. The capacitances obtained at different discharge current densities are illustrated in **Table 1**.

Table 1 Specific capacitances of 60 wt% $Ni(OH)_2$/XC composite discharged at different current densities with AB and CNT as conductive agents.

Electrode \ Current density A g^{-1}	Specific capacitance F g^{-1}			
	1	2	5	10
XC-AB	951	873	715	645
XC-CNT	1560	1205	969	840

From **Table 1**, the capacitances with CNTs as conductive agent are all better than those with AB as conductive agent while discharging at the same current density; with current density increases, the capacitance decreases with either CNTs or AB as conductive agent. So we can draw a conclusion that for 60 wt% $Ni(OH)_2$/XC-72 composite, CNTs is a better conductive agent than AB due to its lower resistance, easier diffusion and transport of electrolyte ions, and more affordable electrochemical active sites involved in the charge/discharge Faradaic reaction. Then XC-CNT will be investigated by CV with various scan rates and galvanostatic charge-discharge at different current densities.

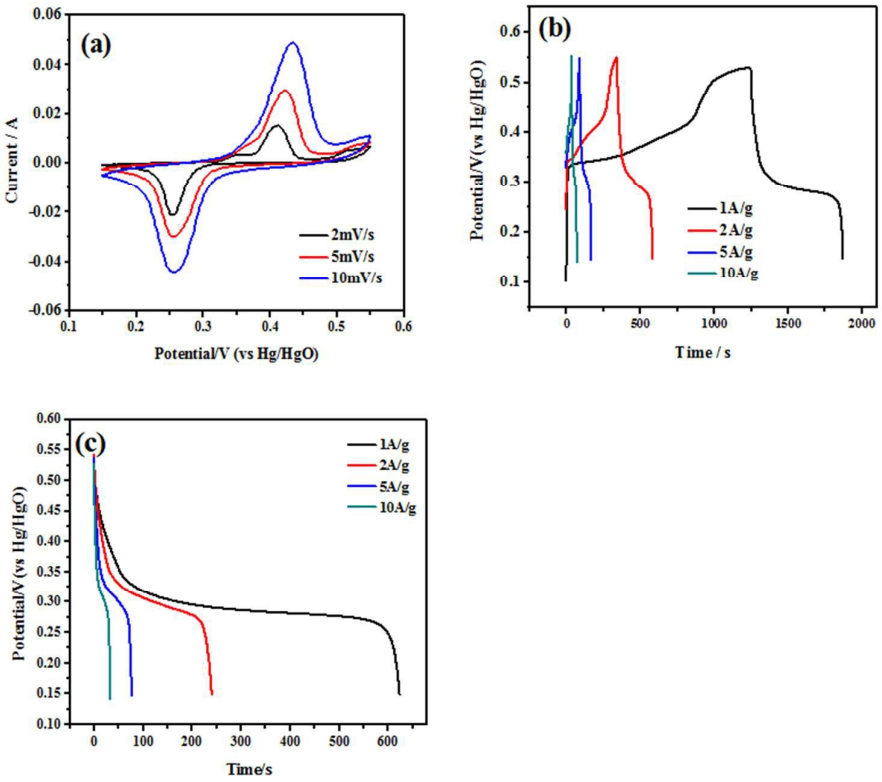

Fig. 7 CV curves of XC-CNT at different scan rates (a). Galvanostatic charge/discharge curves of XC-CNT at various current densities (b). Discharge curves of XC-CNT at various current densities (c).

Fig. 7 shows the electrochemical performances of XC-CNT. CV curves of XC-CNT at various scan rates are shown in **Fig. 7** (a). The pair of redox peaks at 0.41 V and 0.25 V indicating that the capacitance characteristics are mainly governed by Faradaic reaction, which is very distinct from a rectangular shape, produced by a mechanism which electrical energy is stored via a static double electric layer. The two anodic peaks occurred around 0.36 V and 0.41 V (vs Hg/HgO) at scan rate of 2 mV s^{-1}, which can be originated from two oxidation reactions of α-$Ni(OH)_2$ and β-$Ni(OH)_2$ to NiOOH, respectively. While the cathodic peak occurred at around 0.25 V (vs Hg/HgO), should correspond to the reduction reaction of NiOOH to $Ni(OH)_2$. With increase of scan rate, anodic and cathodic peak potentials almost keep unchanged and the I_a/I_b ratio is closed to 1, these indicate that the electrochemical redox reaction $Ni(OH)_2 + OH^- \leftrightarrow NiOOH + H_2O + e^-$ is reversible. The specific capacitances are calculated be to 1296, 1112, and 952 F g^{-1}corresponding to CV scan rates of 2, 5, and 10 mV s^{-1} based on equation (1).

Galvanostatic charge/discharge curves of XC-CNT at various current densities with a potential window between 0.15 and 0.55 V are shown **Fig. 7** (b), and the discharging curves are separately displayed in **Fig. 7** (c) for more direct evaluation of the specific capacitance. The specific capacitances are calculated to be 1560, 1205, 969, and 840 F g-1 at discharging current densities of 1, 2, 5, and 10 A g^{-1} according to equation (2), respectively. The reproducibility researches of XC-CNT are shown in **Fig. S2-Fig. S4**. Three batches of samples were prepared under same parameters, and the standard deviation (SD) and relative standard deviation (RSD) are calculated via the specific capacitances at scan rate of 2 mV s^{-1}, SD and RSD are 47.7 F g^{-1} and 3.7%, respectively. So the reproducibility is good enough to be accepted. Furthermore, the results of this work will be compared with the reported data based on $Ni(OH)_2$ and carbon materials. The details are shown in **Table 2**.

Table 2 Comparison of $Ni(OH)_2$ based on different carbon materials.

Composite	$Ni(OH)_2$ content	Scan rate or Current density	Specific capacitance F g^{-1}	Reference
XC-CNT	60wt%	1 A g^{-1}	1560	This work
XC-CNT	60wt%	2 mV s^{-1}	1290	This work
$Ni(OH)_2$/AC	6 wt%	2 mV s^{-1}	314.5	Ref. 4
α-$Ni(OH)_2$/CNT	66 wt%	0.5 A g^{-1}	1144	Ref. 24
NiAl-LDH/GNS	89.7wt%	1 A g^{-1}	1255.8	Ref. 28
$Ni(OH)_2$/CNT	98.2 wt%	1 A g^{-1}	720	Ref. 36
$Ni(OH)_2$/MWCNT	10 wt%	10 mV s^{-1}	432	Ref. 37

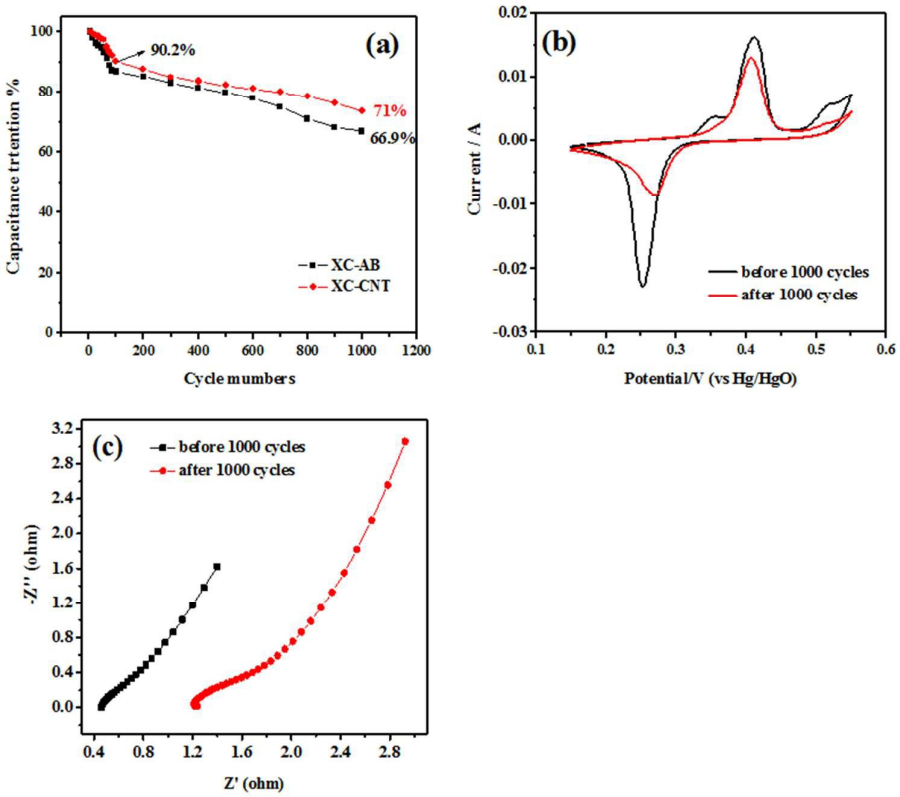

Fig. 8 Stability performance of XC-AB and XC-CNT with a CV scan rate of 100 mV s^{-1} (a). CV curves of XC-CNT electrode before and after 1000 cycles at 2 mV s^{-1} (b). Nyquist plots of XC-CNT sample before and after 1000 cycles (c).

Cycling stability is crucial for a supercapacitor electrode material. For 60 wt% $Ni(OH)_2$/XC-72, it was continuously tested 1000 cycles with a CV scan rate of 100 mV s^{-1}, the specific capacitance was calculated at various cycles, then its cycling stability is recorded in **Fig. 8** (a). The specific capacitance rapidly decreases to ca. 90% after the first 100 cycles, then it reaches relative stable duration, eventually the composite with CNTs as conductive agent shows 71 % capacitance retention after 1000 CV cycles. Then we can draw a conclusion that 60 wt% $Ni(OH)_2$/XC-72 composite demonstrates a relative good stability, mainly because carbon nanomaterial XC-72 possesses relative large specific surface area to assure $Ni(OH)_2$ particles to be distributed uniformly with smaller size, and it also has a large amount of meso-pores and good conductivity to reduce transportation impedance of electrolyte ions and electron during charging and discharging processes. But the composite with AB as conductive agent shows 66.9 % capacitance retention after 1000 CV cycles. Compared to different conductive agents, CNTs indicates better performances of specific capacitance and cycling stability than AB, because CNTs is highly graphitized with better electron conductivity and much bigger respect ratio which facilitate the redox reaction.

After all, the stability decreases nearly 30 percentage after 1000 CV cycles. What factors are contributed to the performance decay? From the CV curves of 60 wt% $Ni(OH)_2$/XC-72 composite before and after 1000-cycle CV test shown in **Fig. 8** (b), the anodic peaks change from two peaks to one peak after life test, the peak at 0.36 V disappeared which means that α-$Ni(OH)_2$ has been totally converted to β-$Ni(OH)_2$ during the cycling test. β-$Ni(OH)_2$ phase is more condense and has less water kept interlayers [38], thus leads to a slower redox reactions and smaller current density, Furthermore, the cathodic current density decays more significantly that the anodic one, it is probably because that H^+ ions are more difficult to diffuse into $Ni(OH)_2$ bulk phase than they move out. Another reason is originated from $Ni(OH)_2$ particles gradual agglomeration at a long charging/discharging duration in the electrical field. This can be proved by SEM images in **Fig. 5**.

EIS is a useful technique to probe mechanism in electrochemistry. For 60 wt% $Ni(OH)_2$/XC-72 composite with CNTs as conductive agent, the experiment was carried out at open circuit potential and potential amplitude of 5 mV in frequency range of 10^5 Hz to 10^{-2} Hz, and its Nyquist plots obtained before and after 1000 CV cycles are displayed in **Fig. 8** (c). After cycling test, Rs increases from 0.5 to 1.2 Ω, this increase is mainly ascribed to change of active material properties such as increment of $Ni(OH)_2$ particle size and phase change as previously mentioned. Moreover, the charge transfer resistance increases obviously due to β-$Ni(OH)_2$ with less interlayer water. However, Warburg resistance decreases slightly, might because of bigger $Ni(OH)_2$ particles with smaller diffusion

resistance. EIS result is in good agreement with SEM images, CV curves, and cyclic stability.

Conclusions

XC-72 is an excellent support for fuel cell catalyst, and is also a good support of $Ni(OH)_2$ for supercapacitor electrode material. Microwave assisted method is a facile and easily scaled-up technique to prepare high performance $Ni(OH)_2$/XC-72 composite. CNTs with good electron conductivity and large respect ratio to construct 3-D interconnected conductive network, it demonstrates better performance than AB as being a conductive agent. XC-CNT exhibits good electrochemical performance of 1560 F g^{-1} at a current density of 1 A g^{-1} and 71% capacitance retention after 1000 CV cycles.

Acknowledgements

This work was supported by Scientific Research Foundation for Returned Scholars, Ministry of Education of China, International Technology Collaboration of Chengdu Science and Technology Division, Technology Project of Education Department of Sichuan Province (13ZA0193), and Innovative Research Team of Southwest Petroleum University (2012XJZT002).

References

1 J. Pu, Y. Tong, S. Wang et al. ***J. Power Sources***, 2014, 250:250-256.
2 X.Y. Chen, C. Chen, Z.J. Zhang et al. ***J. Power Sources*****,**2013, 230: 50-58.
3 L.Yu, G.Q. Zhang, C.Z. Yuan et al. ***Chem. Commun***. , 2013, 49: 137-139.
4 Q. Huang, X. Wang, J. Li et al. ***J. Power Sources***, 2007, 164:425-429.
5 X. Chen, X. Chen, F. Zhang, et al. ***J. Power Sources***, 2013, 243:555- 561.
6 S. J. Kim, G. J. Park, B. C. Kim et al. ***Synth. Met.***, 2012, 161: 2641-2646.
7 P. Kolla, M. Schrandt, R. Cook, et al. ***J. Electrochem. Soc.***, 2014, 3: 160-160.
8 P. Hao, Z. Zhao, J. Tian, et al. ***Nanoscale***, 2014, 20: 12120-12129.
9 P. Simon, Y. Gogotsi, ***Nat. Mater***. , 2008, 7: 845-854.
10 P. M. Kharade, S. G. Chavan, D. J. Salunkhe et al. ***Mater. Res. Bull.*** 2014, 52:37-41.
11 C. C. Hu, K. H. Chang, M. C. Lin et al. ***Nano Lett.*** , 2006,6: 2690-2695.
12 J. Yan, Z. Fan, T. Wei et al. ***Mater. Sci. Eng. B***, 2008, 151:174-178.
13 Y. Zhang, C. Sun, P. Lu et al. ***CrystEngComm.*** 2012, 14 : 5892-5897.
14 S. L. Xiong, C.Z. Yuan, X.G. Zhang et al. ***Chem. Eur. J***., 2009, 15: 5320-5326.
15 X. Dai, D. Chen, H. Fan et al. ***Electrochim. Acta.*** 2015, 154: 128-135.
16 X. Chen, K. Chen, H. Wang et al. ***J. Colloid. Interf. Sci.*** 2015, 44 : 49-57.
17 G. P. Wang, L. Zhang, J. J. Zhang. ***Chem. Soc. Rev.***, 2012, 41:797-828.
18 S. Chen, J. J. Duan, M. Jaroniec et al. ***J. Mater. Chem.A***,2013, 1： 9409-9413.
19 G. A. Snook, P. Kao, A.S. Best. ***J. Power Sources*****,** 2011, 196: 1-12.
20 K. Chen, C. Sun, D. Xue et al. ***Phys. Chem. Chem. Phys.*** 2015, 17: 732-750.
21 D. P. Dubal, S. H. Lee and W. B. Kim, ***J. Mater. Sci.***, 2012, 47: 3817-3821.
22 J. Zhang, S. Liu, G. Pan et al. ***J. Mater. Chem. A***, 2014, 2: 1524-1529.
23 J. Ji, L. Zhang, H. Ji et al. ***J. Am. Chem. Soc.***, 2013, 7:6237-6243.
24 L. Wang, H. Chen, F. Caietal. ***Mater. Lett.*** , 2014, 115:168-171.
25 S. Min, C. Zhao, G. Chen et al. ***Electrochim. Acta***, 2014, 115: 155-164.
26 Y. Tian, J. Yan, L. Huang et al. ***Mater. Chem. Phys.***, 2014, 143:1164-1170.
27 H. Kim, B. N. Popov. ***J. Power Sources***, 2002, 104: 52-61.
28 L. Zhang, J. Wang, J. Zhu et al. ***J. Mater. Chem. A***, 2013, 1: 9046-9053.
29 G. T. Duan, W. P. Cai, Y. Y. Luo et al. ***Adv. Funct. Mater***. 2007,17: 644-650.
30 J. L. Zhang, H. D. Liu, L. H. Huang et al. ***J. Sold State Electrochem***. 2015,19: 229-239.
31 J. Yan, T. Wei, B. Shao et al. ***Carbon***, 2010, 48: 487-493.
32 F. Tuinstra, J. L. Koenig. ***J. Chem. Phys***.1970, 53: 1126-1130.
33 H. Bode, K. Dehmelt, J. Witte et al. ***Electrochim. Acta***, 1966, 11: 1079-1087.
34 D. M. Mac Arthur. ***J. Electrochem. Soc.***, 1970, 117:422-426.
35 P. Lu, F. Liu, D. Xue et al. ***Electrochim. Acta.*** 2012, 78: 1-10.
36 H.Cheng, A. D. Su, S. Li et al. ***Chem. Phys. Lett.***. 2014, 601: 168-173.
37 C. Liu, Y. Lee, Y. Kim et al. ***Synthetic Met.***, 2009,159: 2009-2012.
38 L. Indira, M. Dixit, P.Vishnu et al. ***J. Power Sources*****,** 1994, 52: 93-97.